Petroleum Science 19 (2022) 1664–1673

Contents lists available at ScienceDirect

Petroleum Science

journal homepage: www.keaipublishing.com/en/journals/petroleum-science

Original Paper

Laboratory investigation on hydraulic fracture propagation in sandstone-mudstone-shale layers

Jiang-Chuan He [a], Kuang-Sheng Zhang [a], Han-Bin Liu [a], Mei-Rong Tang [a], Xue-Lin Zheng [b], Guang-Qing Zhang [b, c, *]

[a] PetroChina Changqing Oilfield Company, Xi'an, 710018, Shaanxi, China
[b] College of Petroleum Engineering, China University of Petroleum (Beijing), Beijing, 102249, China
[c] State Key Laboratory of Petroleum Resources and Prospecting, China University of Petroleum (Beijing), Beijing, 102249, China

ARTICLE INFO

Article history:
Received 24 October 2021
Received in revised form
15 March 2022
Accepted 16 March 2022
Available online 23 March 2022

Edited by Yan-Hua Sun

Keywords:
Sandstone-mudstone-shale
Multi-layers
Hydraulic fracturing experiments
Lithological interface

ABSTRACT

During the stimulating unconventional reservoirs, the vertical propagation of hydraulic fractures is crucial for enlarging the stimulated reservoir volume, especially in multi-layers of sandstone, mudstone and shale (sand-mud-shale). To investigate the effects of lithological interface and fracturing fluid viscosity on the fracture propagation vertically in the multi-layers, hydraulic fracturing experiments in laboratory were performed on the outcrop samples of 30 cm × 30 cm × 30 cm collected from Yanchang Formation in Ordos Basin. The results show that hydraulic fractures are multi-branched and zig-zagged when they initiate in shale, simple when they commence in sandstone or mudstone. Hydraulic fractures created with low-viscosity fracturing fluid can only cross sandstone from mudstone, but those induced by high-viscosity fracturing fluid can cross the sand-mud-shale layers. Furthermore, the high-viscosity fracturing fluid reduces the fractures complexity in shale, facilitating vertical fracture propagation. The injection pressure fluctuates slightly as the hydraulic fracture extends from shale to sandstone or mudstone, otherwise it fluctuates significantly. From the laboratory investigation, a hydraulic fracturing scheme for Chang 7 Member was proposed, with its feasibility proved in field tests.

1. Introduction

In recent decades, fracture propagating in multi-layer formations is challenging for stimulating unconventional oil shale reservoirs (Barree et al., 2002; Cipolla et al., 2008). One of the crucial issues happens when hydraulic fractures run across the interbedded layers or multi-layers with various lithologies, such as thin layers of sandstone, mudstone and shale (sand-mud-shale) (Wang et al., 2021). Numerous experimental investigations and field applications show that the inference of the interfaces of lithological layers during hydraulic fracture extension mainly includes: crossing through the interface, arresting at the interface and propagating along the interface (Fisher and Warpinski, 2012; Pan et al., 2021; Thiercelin et al., 1987; Tan et al., 2021). When hydraulic fractures propagate along the interface, a new fracture may initiate at a weak point or the end of the interface of less resistance (Potluri et al., 2005; Tan et al., 2020).

For payzones (such as sandstone) and barriers (such as mudstones) of a large thickness (>5 m), the hydraulic fractures are expected to be contained in the payzones. The laboratory experiments (Warpinski et al., 1982) and mine excavation (Teufel and Warpinski, 1983) show that the difference of horizontal stresses among neighboring layers prevail in determining vertical propagation of hydraulic fractures. If the horizontal stress difference among the interlayers is greater than 4 MPa, hydraulic fractures will hardly penetrate the interface into other interlayers. Besides the *in-situ* stresses, the rock mechanical properties of the layers, such as elastic modulus (El Rabaa, 1987) and interface strength (AlTammar et al., 2019), can as well affect the vertical propagation of hydraulic fractures.

In hydraulic fracturing treatments, it is preferable for hydraulic fractures be contained in the payzone (sandstone), or no significant intrusion into the interlayer (mainly mudstone and shale). However, for multi-payzones of thin thickness, simultaneous fracturing

* Corresponding author. College of Petroleum Engineering, China University of Petroleum (Beijing), Beijing, 102249, China.
E-mail address: zhangguangqing@cup.edu.cn (G.-Q. Zhang).

https://doi.org/10.1016/j.petsci.2022.03.018

of them was proved advantageous over individual fracturing each payzone (Fu et al., 2019; Yang et al., 2013), resulting in an improved treatment efficiency and reduced cost. So maneuvering hydraulic fractures across multiple thin layers to connect more sweet spots is the priority (Mu et al., 2019; Zhao et al., 2018). Experimental investigation, numerical simulation and field tests show that moderate stress difference and mechanical properties between the layers prompt the fracture to extend across the layers (Beugelsdijk et al., 2000; Liu et al., 2014; Pan and Zhang, 2018; Teufel and Clark, 1984). Increasing the injection rate or the viscosity of the fracturing fluid can also contribute to fractures crossing the layers (Fan and Zhang, 2014; Llanos et al., 2017; Zhang et al., 2014; van Eekelen, 1982). In addition, the large interface friction (Anderson, 1981), excessive interfacial strength (Casas et al., 2006), and extensive cohesive area (Fu et al., 2018) can help the cross-layer propagating of hydraulic fractures.

Chang 7 Member in Changqing Oilfield is a typical shale oil reservoir. Conventional horizontal well multi-stage fracturing in this reservoir did not yield satisfactorily, due to the various lithology and thin interbedding, rendering complicated fracture propagation. Therefore, connecting multiple layers with vertical fractures is demanding to improve the fracturing effectiveness. Laboratory experiments of hydraulic fracture propagation in sand-mud-shale complex were carried out to investigate hydraulic fracture propagation, and on-site hydraulic fracturing treatments were suggested.

2. Compositional, microscopic and mechanical properties of sand-mud-shale complex

To characterize the sand-mud-shale complex in Chang 7 Member, the mineral composition, microscopic structure and mechanical properties of the sandstone, mudstone and shale were obtained, and fracture paths were analyzed.

2.1. Mineral composition and microscopic characteristics

The mineral composition averaged on 30 samples of sandstone, mudstone and shale selected from Chang 7 Member was analyzed by XRD, in Fig. 1. A ternary classification was made in terms of QFP (quartz, feldspar, pyrite), carbonates (calcite, dolomite, siderite), and the sum of clay minerals (illite, kaolinite, chlorite and illite-montmorillonite mixed layer) and total organic carbon (TOC). And QFP and carbonates are usually considered as brittle components. According to brittleness indices defined upon the lithologies

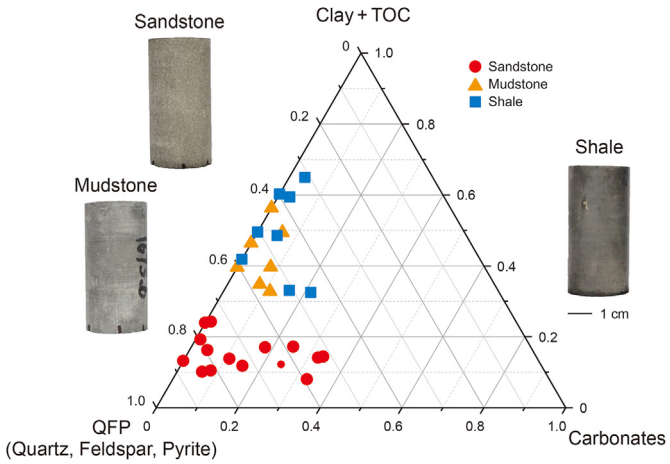

Fig. 1. Composition of sandstone, mudstone and shale of Chang 7 Member.

(Zoback and Kohli, 2019), the content of brittle minerals, the average brittleness for sandstone, mudstone and shale are 0.849, 0.573 and 0.603, indicating that sandstone is the most brittle, followed by shale, and mudstone takes the third position.

The casting thin section is mostly used to analyze features of micro-pores and cracks. As from Fig. 2, there are two micro-fractures in shale and one micro-fracture in both sandstone and mudstone. On a microscopic view, micro-fractures in shale are the most developed. The distribution of pre-existing fractures can affect the hydraulic fractures in different layers, especially in shale, which may be reactivated by hydraulic fracturing to form a complex fracture network.

2.2. Mechanical properties

The mechanical properties of different lithological formations are the basis for designing hydraulic fracturing experiments. The compressive or tensile strength and elastic properties of sandstone, mudstone and shale of Chang 7 Member are obtained with tri-axial compressions with confining pressure of 20 MPa and Brazil tests. From Tables 1–3, for sandstone, mudstone and shale, their compressive strengths are 202.00, 164.34, and 119.02 MPa, the tensile strength 7.41, 6.09, and 5.17 MPa, the elastic modulus 27.71, 25.41, and 22.14 GPa, and Poisson's ratio 0.241, 0.247, and 0.246. The compressive/tensile strengths and elastic modulus of sandstone are higher than those of mudstone and shale, while Poisson's ratio is lower than that of mudstone and shale.

The hydraulic fracture is normally dominated by tensile failures, like tensile fracture in Brazil tests, as shown in Fig. 3, for sandstone, mudstone and shale. It can be found that in sandstone and mudstone a single fracture is created, in Fig. 3(a) and (b). However, several sub-parallel tensile fractures are induced in shale, in Fig. 3(c). Therefore, from the above comparisons, it can be inferred that the hydraulic fractures in shale are more complicated than in both sandstone and mudstone.

3. Specimen preparation and experimental procedure of hydraulic fracturing

Considering interbedding of sandstone-mudstone and shale in Chang 7 Member (Yang et al., 2013; Fu et al., 2019), perforating schemes and fluid injection, we used the Chang 7 outcrops in our experiments to simulate the hydraulic fracture in sand-mud-shale complex for reservoir conditions.

3.1. Specimen preparation

Both sandstone and shale were selected from outcrops, and the mudstone is simulated by concrete with weight ratio of quartz to the cement of 1:1. The selected outcrops were cemented as a sand-mud-shale complex as shown in Fig. 4, and it is found the mechanical properties of the selected outcrop and formation rocks are comparable, hence the outcrop can be reckoned as representative of formation rock (Table 4). As shown in Fig. 4, outcrops of sandstone, shale and mudstone were cut into cuboid blocks of 300 mm × 300 mm × 90 mm, which were cemented into one block of 300 mm × 300 mm × 300 mm. A wellbore 10 mm in diameter and 150 mm deep, is bored, at the bottom of which a notch was pre-cut as the initial fractures. A stainless steel tube was glued in the wellbore for injecting fracturing fluid. The experiments in Table 5 were performed with the large-scale system of hydraulic fracturing under tri-axial stresses.

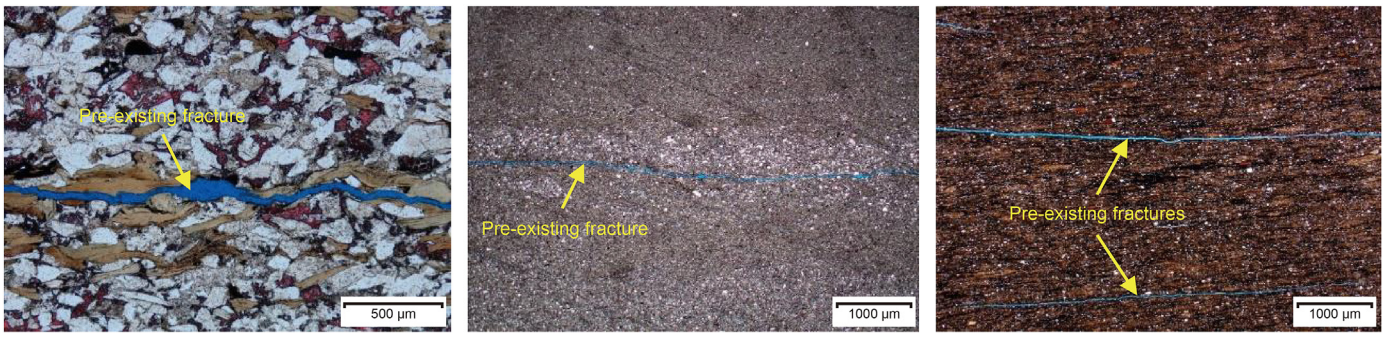

Fig. 2. Microscopic fractures of Chang 7 Member.

Table 1
Mechanical properties of Chang 7 sandstone.

No.	Block	Well	Depth, m	Compressive strength, MPa	Tensile strength, MPa	Elastic modulus, GPa	Poisson's ratio
1–1	S	S-1	2015.60	167.87	9.16	29.55	0.200
1–2	Z	Z-1	1669.90	175.04	8.06	19.95	0.250
1–3	N	N-1	1885.70	175.02	5.92	25.47	0.230
1–4	N	N-1	1916.65	164.10	5.09	27.60	0.220
1–5	N	N-1	1930.45	195.04	7.82	29.16	0.220
1–6	N	N-1	1979.00	224.98	8.36	26.37	0.220
1–7	N-H	N-H-1	2369.40	254.42	7.19	32.01	0.236
1–8	N-H	N-H-1	2380.60	202.11	6.32	28.25	0.227
1–9	M	M-1	2186.20	226.13	7.38	34.48	0.298
1–10	M	M-2	2247.10	203.32	6.87	28.31	0.267
1–11	H	H-1	2414.72	206.69	7.47	26.25	0.280
1–12	H	H-2	2178.00	257.23	8.82	34.58	0.176
1–13	H	H-3	2082.10	222.24	9.63	31.61	0.250
1–14	J	J-1	2155.70	177.62	4.38	18.82	0.308
1–15	Z-A	Z-A-1	1162.20	178.16	8.61	23.29	0.240
Average				202.00	7.41	27.71	0.241

Table 2
Mechanical properties of Chang 7 mudstone.

No.	Block	Well	Depth, m	Compressive strength, MPa	Tensile strength, MPa	Elastic modulus, GPa	Poisson's ratio
2–1	Z	Z-1	1675.60	151.21	4.52	19.03	0.220
2–2	N	N-1	2017.53	174.46	6.74	29.54	0.220
2–3	M	M-1	2212.80	145.50	6.24	20.14	0.255
2–4	H	H-1	2420.30	175.98	5.56	29.15	0.262
2–5	H	H-2	2191.60	115.00	4.34	23.63	0.285
2–6	J	J-1	2222.60	198.04	7.59	29.93	0.276
2–7	Z-A	Z-A-1	1200.70	190.20	7.67	26.48	0.213
Average				164.34	6.09	25.41	0.247

Table 3
Mechanical properties of Chang 7 shale.

No.	Block	Well	Depth, m	Compressive strength, MPa	Tensile strength, MPa	Elastic modulus, GPa	Poisson's ratio
3–1	S	S-1	2004.50	90.88	5.78	18.96	0.230
3–2	Z	Z-1	1706.76	101.49	5.71	22.91	0.250
3–3	N	N-1	1898.50	135.94	4.73	25.02	0.210
3–4	N	N-1	1898.55	117.48	5.20	23.56	0.310
3–5	N	N-1	1904.80	115.17	3.95	24.12	0.290
3–6	N	N-1	1909.80	145.85	5.96	20.77	0.270
3–7	M	M-2	2251.30	134.67	5.71	24.17	0.202
3–8	H	H-3	2102.05	110.66	4.35	17.60	0.208
Average				119.02	5.17	22.14	0.246

Fig. 3. Fractures of sandstone, mudstone and shale in Brazil tests.

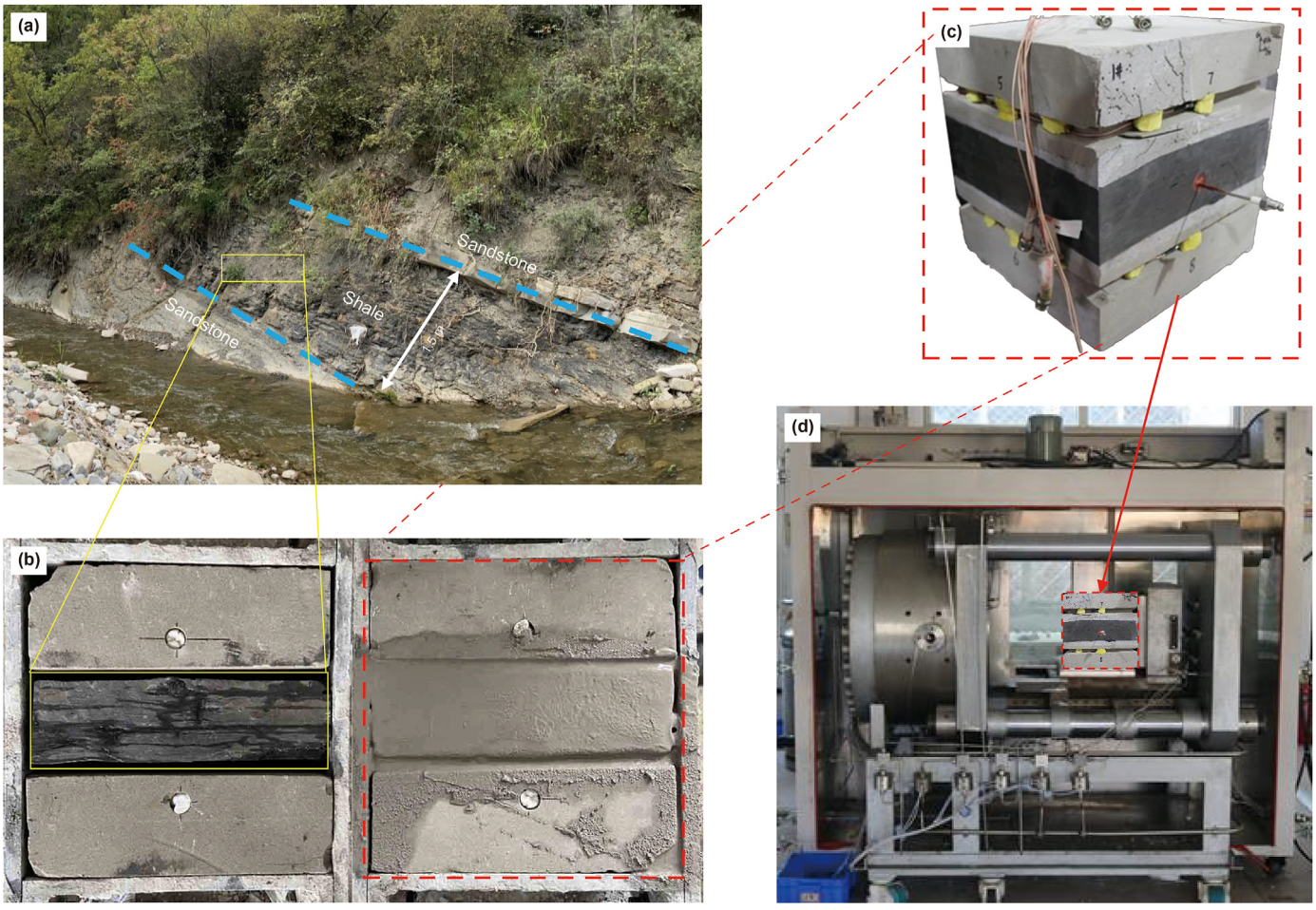

Fig. 4. Specimen preparation and hydraulic fracturing experimental system. (**a**) Sandstone and shale outcrops of Chang 7 Member. (**b**) The shale and sandstone cemented in the mold. (**c**) The finished sand-shale-sand specimen with a borehole in shale. (**d**) The specimen in the hydraulic fracturing system.

Following the lithology features of sand, mud and shale in Chang 7 Member, the perforations can be at sandstone, mudstone or shale, leading to various schemes of fracturing paths. Then, six scenarios of experiments are designed to be the typical models, in Fig. 5, including hydraulic fractures from shale to sandstone, sandstone to shale, shale to mudstone, mudstone to shale, sandstone to mudstone, and mudstone to sandstone.

Table 4
Mechanical properties of outcrop and reservoir rocks of Chang 7 Member.

Rock type	Sandstone			Mudstone			Shale		
	σ_c, MPa	E, GPa	ν	σ_c, MPa	E, GPa	ν	σ_c, MPa	E, GPa	ν
Reservoir rock	226	31.3	0.241	179	27.8	0.247	144	25.7	0.246
Outcrop rock	209	31.0	0.236	147	22.6	0.220	148	28.7	0.205
Similarity, %	92.5	99.0	97.9	82.1	81.3	89.1	97.2	88.3	83.3

Note: σ_c is the tri-axial compressive strength, E elastic modulus, ν Poisson's ratio. Similarity (%) = 100% × (1 − |B − A |/A), A and B represent σ_c, E, and ν of reservoir and outcrop rock.

Table 5
Experimental schemes of hydraulic fracturing.

No.	Fracturing fluid viscosity, mPa s	Lithology distribution	Perforation location	Tri-axial stresses, MPa	Injection rate, mL/min
1-1#	40	Sand-shale-sand	Shale	12/20/25	5
1-2#	230				
2-1#	40	Shale-sand-shale	Sand		
2-2#	230				
3-1#	40	Mud-shale-mud	Shale		
3-2#	230				
4-1#	40	Shale-mud-shale	Mud		
4-2#	230				
5-1#	40	Mud-sand-mud	Sand		
5-2#	230				
6-1#	40	Sand-mud-sand	Mud		
6-2#	230				

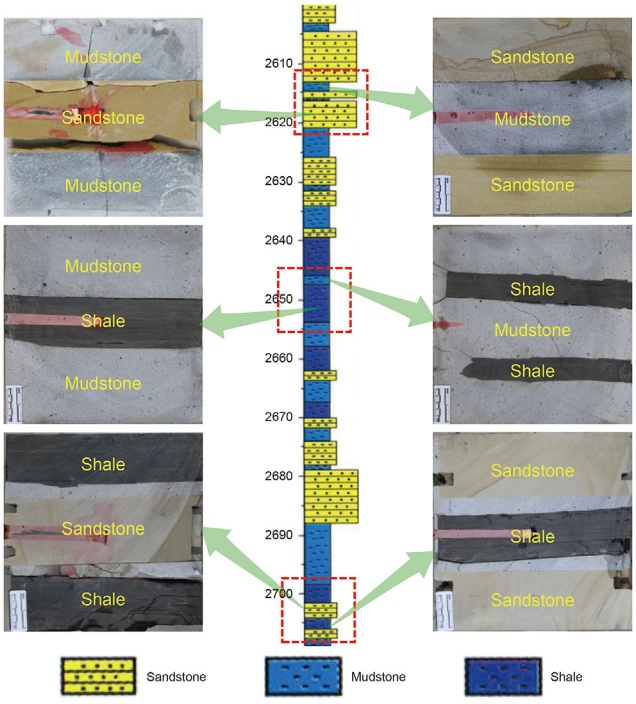

Fig. 5. Six scenarios of sandstone, mudstone and shale from the reservoirs.

3.2. Experimental procedure

In this study, the lithological interface and fracturing fluid viscosity in Table 5, and the controlling experiment parameters, are stemmed from the reservoir geology and fracturing treatment trials. In laboratory tests, the triaxial stresses are inferred from the *in-situ* horizontal stress testing, the viscosity of the fracturing fluid is selected as the on-site fracturing fluid.

The distribution of *in-situ* stress in Chang 7 Member in Ordos Basin (Shi et al., 2014) indicates that the horizontal *in-situ* stress difference ($\Delta\sigma = \sigma_H - \sigma_h$) is from 4 to 8 MPa, and we determined vertical, maximum horizontal and minimum horizontal stresses as 25, 20, and 12 MPa, making stress differences in laboratory work agree with that in the reservoirs. The viscosity of the slickwater used in on-site is below 40 mPa s (Zhu et al., 2013), that with a crosslinking agent is up to 200 mPa s (Sun et al., 2020). Then in the experiments the fluid viscosities of 40 and 230 mPa s are designed for slickwater and gel fracturing fluids. Red dye is added to the fracturing fluid to trace the hydraulic fractures. The injection rate of the fracturing fluid in on-site fracturing is 2–10 m^3/min, the laboratory injection rates are specified as 3–15 mL/min from the similarity law (de Pater et al., 1994; Zhou, 2020), and the injection rate of 5 mL/min is used in our experiments. Twelve specimens are divided into six schemes in Table 5.

4. Experimental results and analysis

Table 6 summarizes the results of six experiment schemes, with changing lithological interface and fracturing fluid viscosity, showing the influence of fracturing fluid viscosity, lithology distribution, perforation location, injection pressure and the interface crossing.

4.1. Effects of the lithological interface on fracturing fracture

When hydraulic fractures initiate in sandstone or mudstone, the fractures in all three layers are single, as in Fig. 6(b), (d), (e), and (f). When the initiations are in shale, the fractures in shale are significantly complicated, in Fig. 6(a) and (c), for low-viscosity fracturing fluids. It is concluded that the vertical extension of hydraulic fractures can be hindered across the interfaces of the multi-fractures, and the hydraulic fractures in sandstone or mudstone are single and simple, but complex in shales. The reason behind may be attributed to the undeveloped micro-fractures in the sandstone or

Table 6
Experimental results of the hydraulic fracturing.

Group	No.	Fracturing fluid viscosity, mPa s	Lithology distribution	Perforation location	Breakdown pressure, MPa	Interface crossing
A	1-1#	40	Sand-shale-Sand	Shale	20.2	N
	1-2#	230			23.7	Y
B	2-1#	40	Shale-sand-shale	Sand	22.9	N
	2-2#	230			33.1	Y
C	3-1#	40	Mud-shale-mud	Shale	25.8	N
	3-2#	230			26.1	Y
D	4-1#	40	Shale-mud-shale	Mud	31.2	N
	4-2#	230			33.9	Y
E	5-1#	40	Mud-sand-mud	Sand	27.0	N
	5-2#	230			31.0	Y
F	6-1#	40	Sand-mud-Sand	Mud	33.6	Y
	6-2#	230			35.5	Y

Note: N for not crossing, Y for crossing.

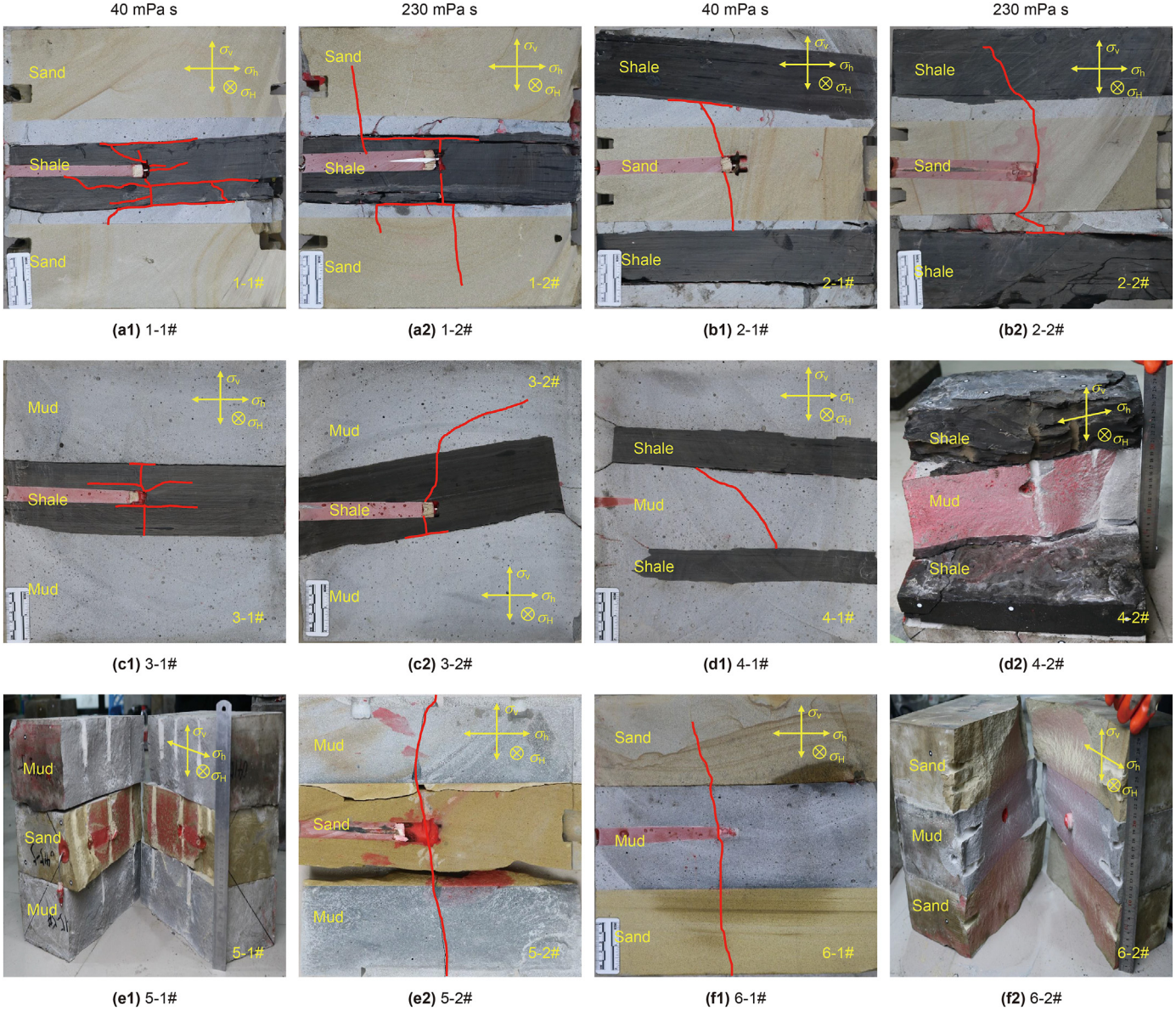

(a1) 1-1# **(a2)** 1-2# **(b1)** 2-1# **(b2)** 2-2#

(c1) 3-1# **(c2)** 3-2# **(d1)** 4-1# **(d2)** 4-2#

(e1) 5-1# **(e2)** 5-2# **(f1)** 6-1# **(f2)** 6-2#

Fig. 6. Hydraulic fractures across the interfaces for two viscosities of fracturing fluids.

mudstone, while to the extensive bedding plane and micro-fractures in shales.

For low-viscosity fracturing fluids, it is worth noting that hydraulic fractures can extend into sandstone when they initiate in mudstone, but contained in the initiation layer in other scenarios. Therefore, initiating in mudstone should be considered to be favorable for fractures propagating vertically for low-viscosity fracturing fluids.

4.2. Effect of fracturing fluid viscosity on fractures

For the samples of sandstone, mudstone, and shale, the breakdown pressures are increased from 25.0, 32.4, and 23.0 MPa at the fluid viscosity of 40 mPa s to 32.1, 34.7, and 24.9 MPa at 230 mPa s. Among them, the breakdown pressure for mudstone is the highest, whereas shale breaks down the most easily.

As in Fig. 6, the viscosity of the fracturing fluid has a significant impact on the vertical propagation of the hydraulic fracture. For the fracturing fluid with viscosity of 40 mPa s, the hydraulic fractures can only penetrate into sandstone from mudstone, however as the viscosity increases from 40 to 230 mPa s, hydraulic fractures can cross multiple layers for all lithologic combinations and initiating layer.

As the viscosity of the fracturing fluid increased from 40 to 230 mPa s, the hydraulic fractures cross as many layers as possible, with significantly reduced fracture complexity, as in Fig. 7. The main reason is that for the fracturing fluid of high viscosity, there will be much increased frictional resistance of the fracturing fluid along with bedding and micro-fractures, whose activation are impeded. Then the reduction of fracture complexity is conducive to the vertical propagation of hydraulic fractures.

In Fig. 8, pressure records were shown for hydraulic fractures from one layer to another among mudstone, sandstone and shale, with the fracturing fluid viscosity of 230 mPa s. These pressure records can help us to infer the fracture extensions inside the samples, comparing with fracture paths in Fig. 6.

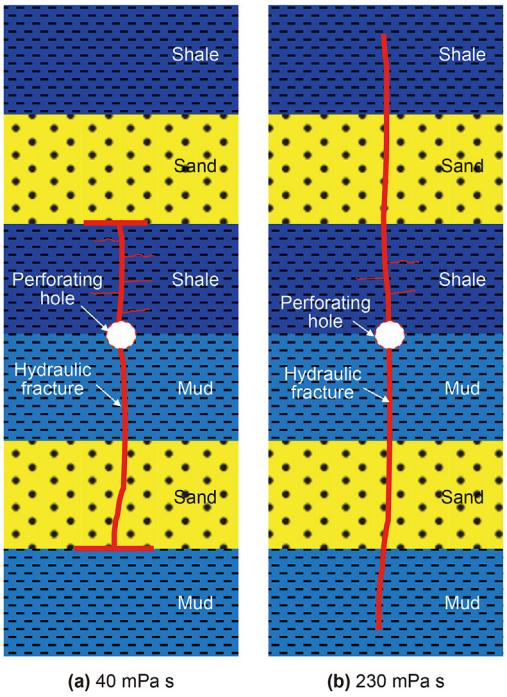

Fig. 7. Diagrams of vertical propagation of hydraulic fractures for two fracturing fluid viscosities.

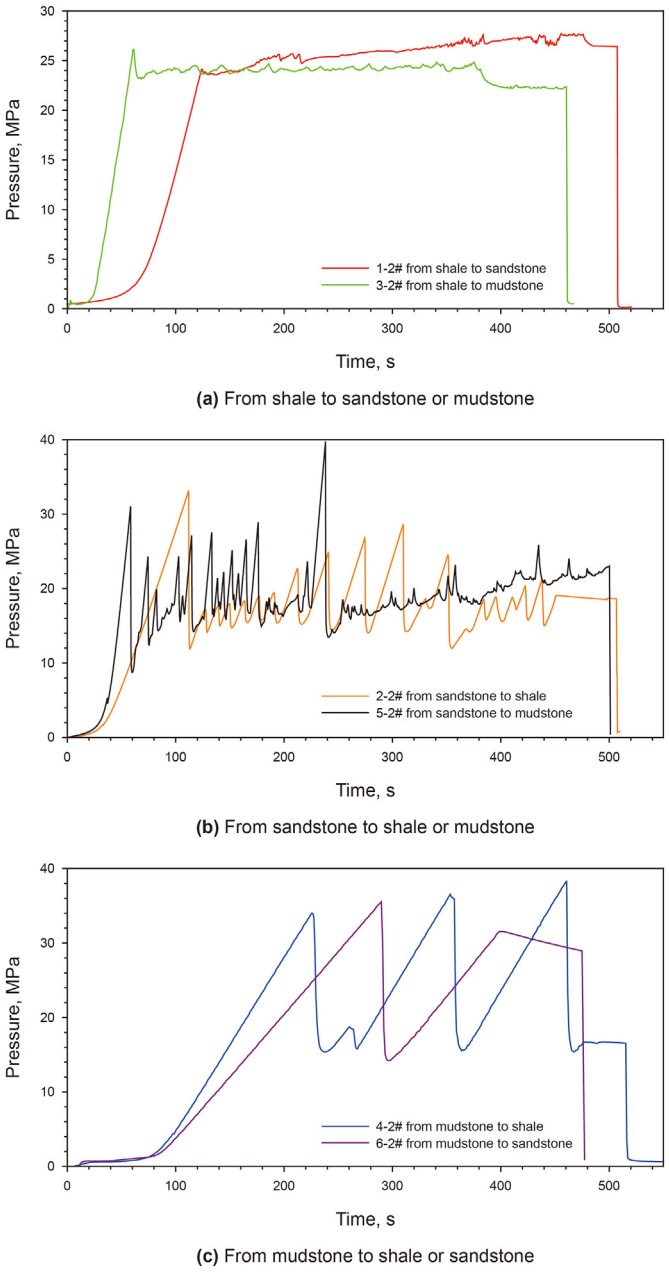

Fig. 8. Injection pressures for initiating layers with the fracturing fluid viscosity of 230 mPa s.

For fractures from shale to sandstone and mudstone, in Fig. 8(a), the pressure records are stable, only with minor fluctuations, suggesting a stable fracture extension. The hydraulic fractures initiate in shales, across it after extending along the interface, into sandstone and mudstone, in Fig. 6(a2) and (c2).

The pressure records for the cases from sandstone to shale and mudstone change abruptly and frequently, as in Fig. 8(b). Though the final fracture seems simple and straight, in Fig. 6(b2) and (e2), scrutinizing red dyes along the interfaces reveals the interfaces were activated multiple times by hydraulic fractures, corresponding to the abrupt fluctuations of injection pressures.

The fluctuations along the pressure records in Fig. 8(c) for those from mudstone to shale and sandstone are in amplitude similar to that in Fig. 7(b), but with less frequency, and the hydraulic

Table 7
Properties of sandstone and mudstone of Chang 7 Member.

Rock	Tensile strength, MPa	Elastic modulus, GPa	Poisson's ratio	Vertical *in-situ* stress, MPa	Minimum horizontal *in-situ* stress, MPa	Maximum horizontal *in-situ* stress, MPa
Sandstone	7.4	27.7	0.241	50	32	40
Mudstone	6.1	25.4	0.247	50	36	44

fractures, in Fig. 6(d2) and (f2), become curved after entering shale and sandstone layers.

5. Suggested fracturing treatments based on lab fracturing

In hydraulic fracturing, perforations were preferably positioned in sandstone other than in mudstone and shale layers. With our laboratory fracturing work, it is found that hydraulic fractures initiated from mudstone can extend into the adjacent sandstone with increased fracturing fluid viscosity, they can penetrate shale to reach sandstone. For the cases of multiple thin sandstones interbedded with thick shale or mudstone, fracturing each sandstone may not be easy and costly, which demands fracturing multiple sandstones at one time, perforating either in mudstone or in shale.

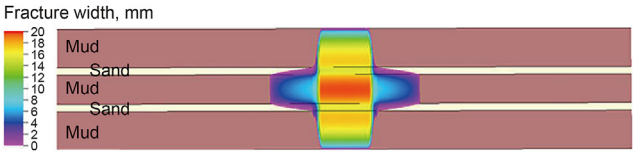

Fig. 9. Simulation results of hydraulic fracture morphology crossing multi-layers.

Conforming Chang 7 Member (Feng et al., 2020), a finite element model is built to simulate fracture extension initiated in mudstone. The properties of sandstone and mudstone are in Table 7, and the fracturing fluid rate and the viscosity are 5 m^3/min and 230 mPa s. The simulated hydraulic fracture from the mudstone to the adjacent sandstone is in Fig. 9, showing that hydraulic fractures initiated from mudstone can propagate into the adjacent sandstone layers, and suggesting a practical fracturing treatment for Chang 7 Member.

Thus, high-viscosity fracturing fluid and perforating in the mudstone and shale are suitable for Chang 7 Member. We integrated such a conclusion into the fracturing scheme of H21-4 well in the Changqing Oilfield, the well trajectory in the reservoir shown in Fig. 10. In fracturing, most stimulation stages are in sandstone, some in mudstone. High-viscosity fracturing is used for all stages. After fracturing, the well produces 20 tons of oil each day, in Fig. 11.

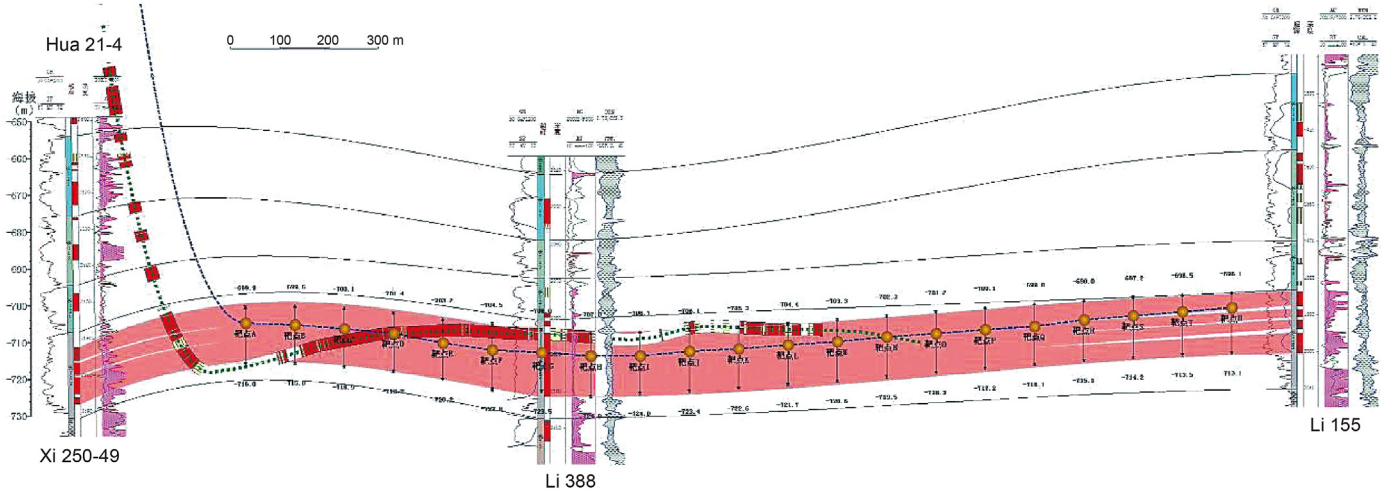

Fig. 10. Perforation positioning along well H21-4 (some parts of the well trajectory are not in sandstone).

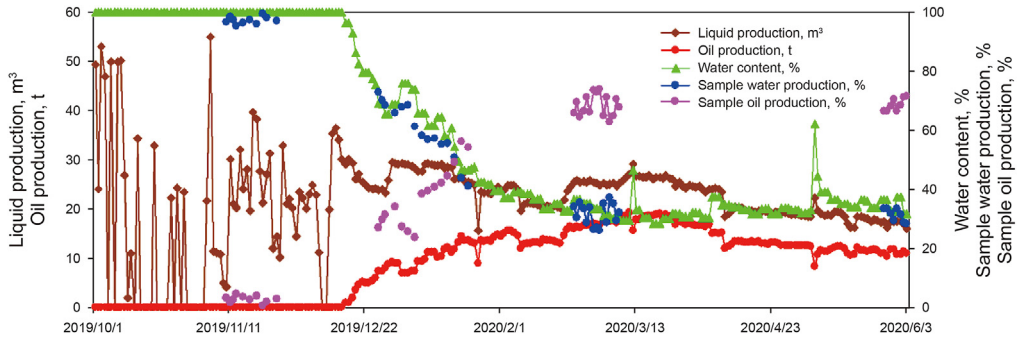

Fig. 11. Production curves of well H21-4.

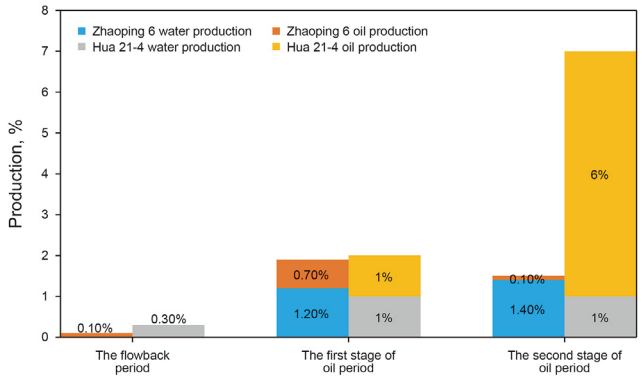

Fig. 12. Production of Hua 21-4 and Zhaoping 6 with initiation in mudstone.

Particularly, for the hydraulic fracturing initiated in mudstone, the production of oil and water is analyzed for the wells Zhaoping 6 and Hua 21-4, in Fig. 12. For the both wells, the fractures are initiated in mudstone, Well Zhaoping 6 with low-viscosity fluid producing oil one sixtieth of Hua 21-4 in the second stage, which was fractured with high-viscosity fluid. This comparison proved the effectiveness of fracturing initiated from mudstone to propagate into the adjacent sandstone with high-viscosity fluid.

6. Conclusions

Based on laboratory experiments, effects of sandstone/shale/mudstone interfaces and fracturing fluid viscosity on hydraulic fractures in sand-mud-shale complex are studied, and a fracturing treatment for Chang 7 Member is proposed and verified by field applications. The main conclusions are as follows:

(1) Hydraulic fractures initiated in mudstone layers can easily extend into the adjacent sandstones. The hydraulic fracture path is complex when it initiates in shale, and is single when it initiates in sandstone or mudstone. This is mainly controlled by the interfaces and natural fractures in shales and sandstones.

(2) Increasing the fracturing fluid viscosity helps hydraulic fractures propagate through multiple layers of sandstone/mudstone/shale. Hydraulic fractures created by low-viscosity fracturing fluid can only extend into sandstone from mudstone, but hydraulic fractures induced by high-viscosity fracturing fluid can cross all the layers of sand-mud-shale. High-viscosity fracturing fluid can also reduce the complexity of fractures in shale.

(3) The injection pressure fluctuates slightly when the hydraulic fracture propagates from shale to sandstone and mudstone, otherwise it fluctuates significantly. This is mainly attributed to multiple interfaces activations and natural fractures.

(4) In Chang 7 Member, high-viscosity fracturing fluid as well as perforating mudstone/shale was recommended to connect sandstones, and proven feasible.

Acknowledgments

This work was sponsored by the Strategic Cooperation Technology Projects of CNPC and CUPB (ZLZX2020-02), the National Science Fund for Distinguished Young Scholars (Grant No. 51925405) and the National Natural Science Foundation of China (Grant no. 51774299).

References

AlTammar, M.J., Agrawal, S., Sharma, M.M., 2019. Effect of geological layer properties on hydraulic-fracture initiation and propagation: an experimental study. SPE J. 24 (2), 757–794. https://doi.org/10.2118/184871-PA.

Anderson, G.D., 1981. Effects of friction on hydraulic fracture growth near unbonded interfaces in rocks. SPE J. 21 (1), 21–29. https://doi.org/10.2118/8347-PA.

Barree, R.D., Fisher, M.K., Woodroof, R.A., 2002. A practical guide to hydraulic fracture diagnostic technologies. SPE Annu. Tech. Conf. Exhib. https://doi.org/10.2118/77442-MS.

Beugelsdijk, L.J.L., de Pater, C.J., Sato, K., 2000. Experimental hydraulic fracture propagation in a multi-fractured medium. SPE Asia Pacif. Conf. Integr. Modell. Asset Manag. https://doi.org/10.2118/59419-MS.

Casas, L.A., Miskimins, J.L., Black, A.D., et al., 2006. Laboratory hydraulic fracturing test on a rock with artificial discontinuities. SPE Annu. Tech. Conf. Exhib. https://doi.org/10.2118/103617-MS.

Cipolla, C.L., Warpinski, N.R., Mayerhofer, M.J., 2008. Hydraulic fracture complexity: diagnosis, remediation, and exploitation. SPE Asia Pacific Oil Gas Conf. Exhib. https://doi.org/10.2118/115771-MS.

de Pater, C.J., Cleary, M.P., Quinn, T.S., et al., 1994. Experimental verification of dimensional analysis for hydraulic fracturing. SPE Prod. Facil. 9 (4), 230–238. https://doi.org/10.2118/24994-PA.

El Rabaa, W., 1987. Hydraulic fracture propagation in the presence of stress variation. In: SPE Annual Technical Conference and Exhibition. https://doi.org/10.2118/16898-MS.

Fan, T., Zhang, G., 2014. Influence of injection rate and fracturing fluid viscosity on hydraulic fracture geometry in coal. J. Chin. Univ. Petrol. (Nat. Sci. Ed.) 38 (4), 117–123. https://doi.org/10.3969/j.issn.1673-5005.2014.04.017 (**in Chinese**).

Feng, Z., Ma, F., Chen, B., et al., 2020. Geology-engineering integration solution for tight oil exploration of Chang-7 Member, Ordos Basin - focusing on scientific well spacing and efficient drilling. Chin Petrol. Explor. 25 (2), 155–168. https://doi.org/10.3969/j.issn.1672-7703.2020.02.015 (in Chinese).

Fisher, M.K., Warpinski, N.R., 2012. Hydraulic-fracture-height growth: real data. SPE Prod. Oper. 27 (1), 8–19. https://doi.org/10.2118/145949-PA.

Fu, J., Niu, X., Dan, W., et al., 2019. The geological characteristics and the progress on exploration and development of shale oil in Chang7 Member of Mesozoic Yanchang Formation, Ordos Basin. Chin Petrol. Explor. 24 (5), 601–614. https://doi.org/10.3969/j.issn.1672-7703.2019.05.007 (**in Chinese**).

Fu, W., Savitski, A.A., Bunger, A.P., 2018. Analytical criterion predicting the impact of natural fracture strength, height and cemented portion on hydraulic fracture growth. Eng. Fract. Mech. 204, 497–516. https://doi.org/10.1016/j.engfracmech.2018.10.002.

Liu, Z., Chen, M., Zhang, G., 2014. Analysis of the influence of a natural fracture network on hydraulic fracture propagation in carbonate formations. Rock Mech. Rock Eng. 47 (2), 575–587. https://doi.org/10.1007/s00603-013-0414-7.

Llanos, E.M., Jeffrey, R.G., Hillis, R., et al., 2017. Hydraulic fracture propagation through an orthogonal discontinuity: a laboratory, analytical and numerical study. Rock Mech. Rock Eng. 50 (8), 2101–2118. https://doi.org/10.1007/s00603-017-1213-3.

Mu, L., Zhao, Z., Li, X., et al., 2019. Fracturing technology of stimulated reservoir volume with subdivision cutting for shale oil horizontal wells in Ordos Basin. Oil Gas Geol. 40 (3), 626–635. https://doi.org/10.11743/ogg20190317 (**in Chinese**).

Pan, R., Zhang, G., 2018. The influence of fracturing energy anisotropy on hydraulic fracturing path in layered rocks. Chin. J. Rock Mech. Eng. 37 (10), 2309–2318. https://doi.org/10.13722/j.cnki.jrme.2018.0461 (**in Chinese**).

Pan, R., Zhang, G., Li, S., et al., 2021. Influence of the fracture process zone on fracture propagation mode in layered rocks. J. Petrol. Sci. Eng. 202, 108524. https://doi.org/10.1016/j.petrol.2021.108524.

Potluri, N.K., Zhu, D., Hill, A.D., 2005. The effect of natural fractures on hydraulic fracture propagation. In: SPE European Formation Damage Conference. https://doi.org/10.2118/94568-MS.

Shi, D., Zhang, B., He, J., et al., 2014. Feasibility evaluation of volume fracturing of Chang-7 tight sandstone reservoir in Ordos Basin. J. Xi'an Shiyou Univ. (Nat. Sci. Ed.) 29 (1), 52–55. https://doi.org/10.3969/j.issn.1673-064X.2014.01.010 (**in Chinese**).

Sun, M., Pan, Y., Wang, T., et al., 2020. Study on application of GTA-GG modified guanidine gum in fracturing fluid and related properties. Appl. Chem. Ind. 49 (8), 2004–2008. https://doi.org/10.16581/j.cnki.issn1671-3206.20200611.004 (**in Chinese**).

Tan, P., Pang, H., Zhang, R., et al., 2020. Experimental investigation into hydraulic fracture geometry and proppant migration characteristics for southeastern Sichuan deep shale reservoirs. J. Petrol. Sci. Eng. 184, 106517. https://doi.org/10.1016/j.petrol.2019.106517.

Tan, P., Jin, Y., Pang, H., 2021. Hydraulic fracture vertical propagation behavior in transversely isotropic layered shale formation with transition zone using XFEM-based CZM method. Eng. Fract. Mech. 248, 107707. https://doi.org/10.1016/j.engfracmech.2021.107707.

Teufel, L.W., Clark, J.A., 1984. Hydraulic-fracture propagation in layered rock: experimental studies of fracture containment. SPE J. 24, 19–32. https://doi.org/10.2118/9878-PA.

Teufel, L.W., Warpinski, N.R., 1983. In-situ stress variations and hydraulic fracture propagation in layered rock-observations from a mineback experiment. The 5th ISRM Congress, Melbourne, Australia.

Thiercelin, M.J., Roegiers, J.C., Boone, T.J., et al., 1987. An investigation of the material parameters that govern the behavior of fractures approaching rock interfaces. The 6th ISRM Congress, Montreal, Canada.

van Eekelen, H.A.M., 1982. Hydraulic fracture geometry: fracture containment in layered formations. SPE J. 22 (3), 341–349. https://doi.org/10.2118/9261-PA.

Warpinski, N.R., Clark, J.A., Schmidt, R.A., et al., 1982. Laboratory investigation on the effect of in situ stresses on hydraulic fracture containment. SPE J. 22, 333–340. https://doi.org/10.2118/9834-PA.

Wang, Y., Hou, B., Wang, D., et al., 2021. Features of fracture height propagation in cross-layer fracturing of shale oil reservoirs. Petrol. Explor. Dev. 48 (2), 1–9. https://doi.org/10.1016/S1876-3804(21)60038-1, 2021.

Yang, H., Li, S., Liu, X., 2013. Characteristics and resource prospects of tight oil and shale oil in Ordos Basin. Acta Pet. Sin. 34 (1), 1–11. https://doi.org/10.7623/syxb201301001 (**in Chinese**).

Zhang, F., Nagel, N., Sheibani, F., 2014. Evaluation of hydraulic fractures crossing natural fractures at high angles using a hybrid discrete-continuum model. In: The 48th U.S. Rock Mechanics/Geomechanics Symposium.

Zhao, X., Zhou, L., Pu, X., et al., 2018. Geological characteristics of shale rock system and shale oil exploration breakthrough in a lacustrine basin: a case study from the Paleogene 1st sub-member of Kong 2 Member in Cangdong sag, Bohai Bay Basin, China. Petrol. Explor. Dev. 45 (3), 361–372. https://doi.org/10.11698/PED.2018.03.01 (in Chinese).

Zhou, D., 2020. The Influence of Supercritical CO_2 Phase Change on Growth of Multiscale Fractures. Ph.D. Dissertation. China University of Petroleum (Beijing), doi:10.27643/d.cnki.gsybu.2020.000140 (in Chinese).

Zhu, J., Zhang, G., Qiao, G., et al., 2013. The application ang reach of slickwater in shale gas fracturing. Petrochem. Ind. Appl. 32 (11), 24–28. https://doi.org/10.3969/j.issn.1673-5285.2013.11.007 (in Chinese).

Zoback, M.D., Kohli, A.H., 2019. Unconventional Reservoir Geomechanics: Shale Gas, Tight Oil, and Induced Seismicity. Cambridge University Press, Cambridge, pp. 31–86.